NASA Technical Memorandum 83626

Review of the Effects of Microstructure on Fatigue in Aluminum Alloys

Jack Telesman
Lewis Research Center
Cleveland, Ohio

April 1984

NASA

REVIEW OF THE EFFECTS OF MICROSTRUCTURE ON FATIGUE IN ALUMINUM ALLOYS

Jack Telesman

National Aeronautics and Space Administration
Lewis Research Center
Cleveland, Ohio 44135

SUMMARY

Literature survey was conducted to determine the effects of different microstructural features and different load histories on fatigue crack initiation and propagation of aluminum alloys. Comparison of microstructure and monotonic and cyclic properties between powder metallurgy (P/M) and ingot metallurgy (I/M) alloys is presented. The two alloys that are representative of each process on which the comparison is focused are X7091 and 7050.

Included in the report is a detailed description of the microstructure produced through the P/M and I/M processes. The effect of each pertinent microstructural feature on monotonic and cyclic properties, such as yield strength, toughness, crack initiation and propagation is discussed. Also discussed are the proposed mechanisms for crack initiation and propagation, as well as the effects of aggressive environments on these cyclic properties. Included is a discussion of the effects of variable amplitude loading on fatigue crack propagation and the various models proposed to predict load interaction effects.

1. Introduction

The continuous evolution of the military and civilian aircraft structures has lead to significant improvements in the aircraft performance. However, the improvements in the design characteristics of the newly developed aircraft structures are limited by the properties of the presently used materials. Thus, there exists a well-defined need to understand and improve the properties of currently used aircraft materials.

In recent years, the main focus in aluminum alloy development for aircraft structures has centered on both P/M alloys as well as optimization of composition of I/M alloys. Two of the best known new alloys developed by these processes are P/M X7091 and I/M 7050. Due to differences in processing, they have very different microstructures (e.g., grain size, inclusion, dispersoid and oxide composition and distribution). Significant amount of research has been performed recently in order to obtain a better understanding of the effects of different microstructures on both monotonic and cyclic properties of metallic materials in general, and aluminum alloys in particular.

Implementation of the newly developed alloys and processes into advanced aircraft structures requires a careful characterization of cyclic properties such as fatigue crack initiation and propagation. Much effort has been expended in order to attempt to understand and predict fatigue crack propagation rates which are subject to variable amplitude loading.

However, literature search revealed no comprehensive source of information readily available which reviewed all these pertinent areas of ongoing research. Thus, this detailed literature review was developed to fill this niche. It is intended not only to help ongoing research, but also to point out areas where further work is required.

2. Discussion

2.1 History of Alloy Development

2.1.1 I/M 7050

Ingot metallurgy (I/M) alloy 7050 comes from a long line of 7XXX precipitation hardened aluminum alloys based on the Al-Zn-Mg-Cu system. The best known and the most frequently utilized alloy of this series is 7075.

Until the 1960's, the 7XXX alloys were used strictly in the T6 temper (peak aged). The high strength to weight ratio of the 7XXX alloys made them popular with designers, but exfoliation corrosion and stress corrosion problems created intolerable maintenance problems when these alloys were used in the T6 temper (ref. 1).

An overaged heat treatment (T73) was identified in 1960 which substantially alleviated the stress corrosion problems, however the corresponding alloy strength was significantly reduced. In addition, 7075-T73 alloy suffers from relatively poor fracture toughness and high quench sensitivity meaning the inability to retain both strength and ductility in the mid-thickness sections of thick rolled or forged products (ref. 1). However, the properties of 7075-T73 alloy were adequate to make it the dominant alloy of the 1960's and 1970's for aerospace applications.

The rapid progress in the designing of more advanced aircraft structures places an increasingly larger demand on improvements of material properties. Thus, the development of new high strength I/M aluminum alloys in the past fifteen years has been focused on improvement in the following areas (ref. 1):

1. Provide high resistance to stress corrosion cracking (SCC) in the short transverse direction of thick products.

2. Produce thick plates and forgings which will retain high strength and ductility.

3. Improve toughness and short-transverse ductility while maintaining high strength.

4. Improve fatigue crack growth (FCG) resistance without sacrificing other properties.

Researchers at Alcoa Laboratories, in conjunction with Navy and Air Force personnel developed alloy 7050 to meet the above criteria (ref. 2). The quench rate sensitivity of this alloy was improved, thus allowing thick sections to be produced while retaining high strength and ductility (refs. 2 and 3). Better fracture toughness, increased resistance to stress corrosion

cracking (SCC) and slower fatigue crack growth (FCG) rates were obtained for the 7050-T73 alloy in comparison to 7075-T73. A detailed description of the microstructural characteristics of the 7050 alloy as well as the postulated mechanisms responsible for improvement of the critical properties of this alloy are found further on in this section.

The optimization of alloying elements in order to maintain high strength as well as the other improved properties, has resulted in a nominal composition of 7050 as Al-6.2Zn-2.3Mg-2.3Cu-0.1Zr.

As a result of these improvements, 7050 has been widely accepted by aircraft manufacturers, and has already replaced 7075 as the main structural alloy on such advanced aircraft as Navy's F-18.

2.1.2 X7091

An alternative method of producing high strength aluminum alloys is through the utilization of powder metallurgy (P/M) process. In addition to substantially greater alloying freedom, this process offers excellent mechanical properties, superior SCC resistance, a fine homogenous microstructure and absence of large, brittle intermetallic inclusions.

Some of the early work in the development of this process and the applicable alloy compositions was performed by Roberts (refs. 4 and 5). Among the 110 Al-Mn, Al-Mg, Al-Mg-Cu and Al-Zn-Mg-Cu alloy compositions, he found that only Al-Zn-Mg-Cu alloys, containing more Zn and Mg than commercial I/M alloys, offered higher strength than those of the strongest commercial alloys.

Important improvements to the P/M process were made by Towner (ref. 6). He developed a process by which prealloyed atomized powders could be made into extrusions, free of blistering and voids, with longitudinal and transverse elongation equal to those of a comparable I/M product. He also found that the Al-Zn-Mg-Cu system was the most promising for producing superior P/M alloys. In addition he found that alloys containing Co and Fe + Ni were more resistant to grain coarsening during fabrication than those with Cr, Ti, V, Zr, Mo and W additions.

Haarr (ref. 7) found that Al-Zn-Mg-Cu alloys containing Co or Fe + Ni had better combinations of strength and SCC resistance than commercial I/M extrusions. In an effort to optimize the mechanical properties of the P/M alloys, Cebulak (ref. 8) identified a composition of Al-6.5Zn-2.4Mg1.6Cu-0.4Co. This alloy is presently known as X7091 (previously termed MA87 and CT91). The final processing optimization of this alloy was performed by Otto (ref. 9).

A more detailed description of the microstructural characteristics, P/M process, and the mechanisms controlling mechanical properties is found further on in this section.

2.2 Processes

The high strength aluminum alloys, utilized presently in aircraft structures, are produced through the I/M process. The process is typified by melting and alloying, casting into a large relatively slow cooled ingot,

homogenizing the ingot and fabricating the desired products. The slow cooling rates during casting of approximately 0.1 to 1 K/sec (ref. 3) result in a coarse microstructure and large constituent particles. The dendritic cell size (DCS) of cast ingots is approximately 50 μm (ref. 10).

One of the more promising alternate approaches of producing high strength aluminum alloys is the emergence of P/M process. The major reason for using P/M instead of I/M processing is that much higher solidification rates can be obtained. The typical solidification rates for atomized powders are 10^5-10^6 K/sec (ref. 11). Rapid solidification results in significantly finer DCS, and due to supercooling, considerably less precipitation of undissolved particles than the cast structure. The DCS has been measured (refs. 10 and 11) to be from 0.5 to 2.5 μm, and is thus more than an order of magnitude smaller than the DCS for the cast structure. Alloying flexibility is gained since large amounts of alloying elements can be added without macrosegregation (ref. 12).

P/M methods also eliminate other problems encountered in manufacturing large ingots such as cracking due to high thermal stresses during casting, cooling and homogenizing. Very long homogenizing times which are required in materials having coarse DCS are not necessary when the P/M process is applied (ref. 10).

The P/M process (schematically shown in fig. 1), as optimized by Otto (ref. 9), consists of melting and alloying, followed by air atomization to achieve an average particle diameter of 15 μm. The resultant powder is cold isostatically pressed at 207 MPa (30 ksi) into cylindrical compacts having a theoretical density of approximately 70 percent. The compacts are encapsulated in a welded aluminum alloy can. The compacts are hot vacuum degassed at 521° C (970° F) under a vacuum of 35 mm Hg, sealed and hot compacted at a pressure of 620 MPa (90 ksi) to >99.9 percent theoretical density. After the can is removed, the compacts can subsequently be hot worked and aged to a final desired product and temper.

2.3 Physical Metallurgy

2.3.1 Precipitation Reactions

Both of the alloys to be evaluated in this program are based on the Al-Zn-Mg-Cu alloy system. Early work by Mondolfo (ref. 13) identified the age hardening sequence in this system to be:

$$\alpha \text{ solid solution} \rightarrow \text{spherical G.P. zones} \rightarrow \eta' \rightarrow \eta\ (MgZn_2) \qquad (1)$$

where G.P. zones = Guinier Preston zones.

The intermediate transition phase η' has a hexagonal close packed structure with lattice constants of a = 4.69 Å and c = 8.68 Å. The equilibrium phase $MgZn_2$ also has a hexagonal close packed structure with lattice constants: a = 5.15 Å and c = 8.48 Å. A more recent study of aging kinetics by Lyman and VanderSande (ref. 14) revealed an extra step in the precipitation reaction identified as the formation of spherical ordered, hexagonal zones. This newly identified precipitation step follows formation of spherical G.P. zones. The shape of the metastable η' phase is platelike, while the η

phase is in the shape of rod or lath-like particles. The particles undergo coarsening at the rate of:

$$r \propto t^{1/3} \qquad (2)$$

at 150° C (ref. 14).
where
r = particle radius
t = time

G.P. zones nucleate homogenously, and the different precipitates develop sequentially within the matrix. The presence of high angle boundaries and low angle subgrain boundaries may alter the free energy to such as extent that heterogenous nucleation may occur (ref. 15).

In changing from G.P. zones to η during aging, coherency between the matrix and precipitates progressively disappears. G.P. zones are coherent, whereas η' is semicoherent and η is incoherent (ref. 16). Sanders et al. (ref. 17) has shown that metastable phase, η', nucleates directly on dislocations and subgrain boundaries, while the equilibrium η phase nucleates on grain boundaries. A more clear explanation of the nucleation mechanism of η' and η phases emerges from work done by Smith and Grant (ref. 18). They suggested that below G.P. solvus temperature, the G.P. zones act to homogenously nucleate η' and η, however at temperatures above G.P. solvus, the nucleation of η' and η can only occur on dislocations or grain boundaries.

Copper additions to the Al-Zn-Mg system are made in order to increase strength and decrease the susceptibility of the alloys to SCC (ref. 16). A study by Sanders and Starke (ref. 19) revealed that copper raised the critical temperature for homogenous decomposition by increasing the G.P. solvus temperature in comparison to a ternary Al-Zn-Mg alloy. Thus copper stimulates homogenous precipitation in the matrix, thereby reducing the size of the precipitate free zones (PFZ) at the grain boundaries.

2.3.2 Formation of PFZ

Formation of PFZ and grain boundary precipitation are important characteristics of some Al-Zn-Mg alloys.

Two mechanisms have been postulated to explain the formation of PFZ (ref. 20):

1. Vacancy-Depletion. It was postulated that the excess vacancies in the region adjacent to the grain boundaries migrate to the grain boundaries, which are sinks for vacancies. These regions have therefore a lower concentration of vacancies than the balance of the grain. Hence, a precipitate-free but solute-rich region exists adjacent to the grain boundaries.

2. Solute-Depletion. It was proposed that the grain boundary precipitate depletes the adjacent grain regions of solute atoms and thereby lowers the solute supersaturation, hence precipitation is prevented in these regions.

Work by Smith and Grant (ref. 18) indicated that below the G.P. zone solvus, both of these mechanisms can be involved in the formation of PFZ, while for aging temperatures above the G.P. solvus, the vacancy depletion mechanism is responsible for formation of PFZ.

Because of the nature of the grain boundary, the incoherent η can precipitate directly at these interfaces (ref. 16). In addition to grain boundaries, the η particles can also act as sinks for vacancies, thus decreasing the vacancy distribution near grain boundaries and increasing the size of PFZ. To a limited extent the precipitation of the η phase at the grain boundaries can be minimized by rapid quench rate. Thus, if a rapid quench rate is utilized, followed by an aging sequence where precipitation of G.P. zones throughout the matrix is maximized, a material with a narrow PFZ can be formed.

2.3.3 Particle Types and Their Effect

The 7XXX series I/M alloys, such as 7050, contain three types of second phase particles: (1) precipitates, (2) dispersoids, and (3) constituents. These particles influence both the mechanical and physical properties of the material. The powder metallurgy X7091 alloy does not contain large constituent particles, but it does contain, in addition to dispersoids and precipitates, a significant amount of oxide particles.

Constituent particles are large (1 to 30 μm), brittle and are formed during the solidification by the combination of the impurity elements Fe and Si with Al and the solute elements (refs. 1 and 17). The composition of the constituent particles has been identified as Al_7Cu_2Fe and Mg_2Si (ref. 17).

In addition to having these insoluble particles, most high strength I/M aluminum alloys contain intermetallic constituents such as Al_2CuMg (ref. 21) which are at least partially soluble and may be as large as the insoluble particles.

Reduced concentrations of impurity elements Fe and Si decrease the volume fraction of the constituent particles. For instance, low Fe and Si content commercially processed 7050, was found to have a 0.3 percent volume fraction of constituent particles (ref. 21), while a high Fe and Si content commercially processed 7178, contained 4.8 percent of these particles (ref. 22). Sanders and Starke (ref. 21) also reported that the cooling rate plays an important role in determining the volume fraction of the constituent particles. In their study, a slowly cooled 7050 alloy which underwent intermediate thermomechanical treatment (ITMT) contained 1.8 percent constituent particles, while rapidly cooled, commercially processed 7050 of the same composition contained only 0.3 percent of these particles.

Due to high cooling rates, the constituent particles are not formed in the P/M X7091 alloy.

Dispersoid Particles

A second class of smaller particles (0.02 to 0.5 μm), called dispersoids, forms by solid state precipitation of Cr (in 7075), Zr (in 7050) and Co (in X7091) (refs. 10 and 17). The primary role of all the dispersoids is to control grain growth and prevent recrystallization from occurring.

In the case of I/M alloys, the additions of Cr and Zr are retained in supersaturated solid solution during solidification, but they precipitate out during the preheat treatment (ref. 1) as $Al_{12}Mg_2Cr$ and Al_3Zr dispersoid particles. Sanders and Otto (ref. 11) have suggested that in the case of P/M X7091, the Co_2Al_9 dispersoids are formed during powder solification and are probably not affected by subsequent processing.

The $Al_{12}Mg_2Cr$ dispersoids, found in 7075 alloy, are approximately 0.1 μm in diameter and are incoherent with no fixed orientation relationship with the matrix (ref. 17). In contrast, Al_3Zr dispersoids, present in 7050, are coherent spherical precipitates with a diameter of approximately 0.05 μm and a cube/cube orientation relationship with the matrix. These dispersoids are distributed throughout the matrix (ref. 17).

The Al_3Zr particles inhibit but do not completely suppress recrystallization. Sanders and Starke (ref. 21) found that approximately 40 percent of the commercially processed 7050 alloy underwent recrystallization.

Staley (ref. 2) and Thompson et al. (ref. 3) indicated that a replacement of $Al_{12}Mg_2Cr$ dispersoids found in the typical 7XXX series alloys, such as 7075, by Al_3Zr dispersoids will significantly reduce quench sensitivity of the 7050 alloy. Thus, 0.1 percent Zr was added to the composition of 7050 allowing thick yet strong I/M products to be cast.

Since the solubility of Co in aluminum is negligible (ref. 23), only through rapid solidification P/M process could the Co_2Al_9 particles precipitate out as fine dispersoids in the X7091 alloy. The Co_2Al_9 particles are spherical and range in size from 0.1 and 0.5 μm. They are extremely effective in preventing recrystallization and grain coarsening as was shown by Sanders and Otto (ref. 11). In their study 0.4 percent Co in X7091 resulted in an almost completely unrecrystallized structure. The excellent SCC resistance properties of X7091 were partly attributed by Otto (ref. 9) to the Co_2Al_9 dispersoids which are the most cathodic of all phases present and thus may reduce stress corrosion attack by inhibiting formation of atomic hydrogen.

Skinner et al. (ref. 24) suggested that the Co_2Al_9 dispersoids aid in promoting nucleation of G.P. zones.

Hardening Precipitates

Age hardened precipitates are in the form of G.P. zones, η' and η phases. The size of the precipitates ranges from 0.001 μm for G.P. zones to about 1 μm for course, η type, grain boundary precipitates formed during slow cooling or drastic overaging (ref. 1). No noticeable difference has been observed between hardening precipitates in the 7XXX I/M and P/M alloys. The

character and microstructure of the precipitates has already been described in this section.

Oxide Particles

The metal powders, utilized in the processing of X7091, are produced by air atomization and are very fine with the average particle diameter (APD) being ~15 μm (ref. 11). Auger analysis of the powders by Otto (ref. 9) revealed that the two main surface oxides formed during atomization are Al_2O_3 and MgO. The depth of both surface oxides was measured to be from 50 to 100 angstroms. During compaction, the oxide layer breaks up resulting in fine oxide particles (0.01 to 0.04 μm) dispersed throughout the matrix (ref. 10). The oxides are most often found as clusters of stringers in the matrix or at grain boundaries (refs. 10 and 11).

2.3.4 Grain Size

The average grain size of the 7050 alloy has been measured to be 30 μm wide by 100 μm long in the longitudinal direction (ref. 17). It has been reported that approximately 40 percent of the commercially processed 7050 is recrystallized (ref. 21). In the unrecrystallized regions, recovery has for the most part taken place, resulting in the formation of fine, low angle boundary subgrains (ref. 21).

The grain size of P/M X7091 alloy has been measured to be from 1 to 15 μm (ref. 11) and is thus an order of magnitude smaller than that of comparable 7XXX I/M alloys. Low angle subgrain boundaries have also been noted in the X7091 alloy (ref. 12) even though the structure has been reported to be almost fully unrecrystallized (ref. 11).

2.4 Effect of Microstructure on Monotonic and Cyclic Properties

An extensive amount of work has been performed in an effort to understand the influence of microstructural characteristics and the test environment on monotonic and cyclic properties. The most important monotonic properties being investigated are strength, toughness and resistance to SCC, while the research on cyclic properties has been focussed on crack initiation and propagation.

2.4.1 Strength

The increase in strength of age-hardenable aluminum alloys over that of the pure metal is due to the interaction of dislocations with precipitates (ref. 25). The primary strengthening agents in 7XXX alloys are G.P. zones, η' and η precipitates (ref. 21). For the maximum strength temper, T6, these partially coherent phases are penetrated by dislocations during plastic flow. As the particles grow, coherency strains build up and thus increase the strength of the alloy by increasing the stress required for the dislocations to penetrate the particles. For this cutting mechanism, the critical resolved shear stress (CRSS), τ, can be represented by an equation of the form (ref. 25):

$$\tau = cf^{m}r^{p} \qquad (3)$$

where
c = alloy constant depending on particular strengthening mechanism
f = volume fraction of precipitates
r = particle radius
m,p = positive exponents.

The strength increases according to this relationship with both volume fraction and particle size.

Further aging past the T6 temper results in loss of coherency to a point where transformation of η' to η occurs and the precipitates become incoherent (ref. 16). This is accompanied by a change in particle-dislocation interaction from shearing to dislocation looping mechanism termed Orowan hardening. For this mechanism the CRSS can be represented by (ref. 26):

$$t = \frac{0.8Gb\sqrt{f}}{2n[2(1-\nu)r]^{1/2}} \ln \frac{1.6r}{r_o} \qquad (4)$$

where
G = shear modulus
b = Burgers vector
v = Poisson's ratio
r_o = inner cut off ratio of dislocation
r = particle radius
f = volume fraction of precipitates.

Consequently the strength increases with a volume fraction of particles. A double aging treatment used to obtain stress corrosion resistant T73 temper, results in a incoherent particle radius of 40 Å, whereas single aging treatment to achieve the same temper results in η and η' particles having radii of 80 Å and lower tensile strength (ref. 25).

Sanders and Starke (ref. 19) found that in Al-Zn-Mg type alloys, homogenous deformation occurs in the early stages of aging. This fact was attributed to the small resistance to dislocation motion offered by these very small precipitates. Upon further aging the deformation was localized on narrow slip bands parallel to {111} planes.

In an effort to increase the strength of 7XXX alloys in the T6 temper, Ludtka and Laughlin (ref. 27) studied the effect of increasing the volume fraction of strengthening precipitates. They showed that the increase in strength with higher volume fraction of precipitates is associated with coarsening of slip bands and an increase in the slip step height. The increased localization of slip with the higher volume of precipitates might result in decrease in ductility and toughness.

The dispersoid phases are thought to only slightly contribute to the strength while the brittle intermetallics do not contribute to the strength of the alloys (ref. 16).

The reduction in the grain size of the order of magnitude for P/M X7091 in comparison to 7075 resulted in an increase in strength of only 5 to 10 percent (ref. 9). This lack of a pronounced Hall-Petch effect has been attributed (ref. 21) to the fact that G.P. zones, η' and η phases are

primarily responsible for strengthening in these types of alloys. The small grain size of P/M alloys is still very large in comparison to the spacing of precipitates, and thus grain refinement has consequently only a minor strengthening effect.

Thermomechanical treatments (TMT) offers different method of achieving high strengths. TMT includes both intermediate thermomechanical treatments (ITMT) and final thermomechanical treatments (FTMT). The FTMT processing normally consists of solution heat treatment, quench, preaging, cold or warm work, and final aging. The dislocation structure introduced during the working operation is stabilized by heterogenous precipitation during final aging. The FTMT have produced increased strength levels in 7XXX materials (ref. 28).

The ITMT involves specialized ingot processing techniques prior to the final working operation. It is primarily used to control grain structure and dispersoid size and distribution. Sanders and Starke (ref. 21) showed that ITMT results in almost completely recrystallized grain structure which leads to a small increase in tensile strength.

2.4.2 Fracture Toughness

It has been well established (refs. 16, 21, 29, and 30) that second phase particles act as crack initiators and thus are detrimental to the fracture toughness of aluminum alloys. These large (up to 30 μm) particles are primarily insoluble iron and silicon rich intermetallics (Al_7Cu_2Fe, Mg_2Si) and partially soluble intermetallics such as Al_2CuMg.

The coarse, brittle, secondary intermetallic particles fracture or separate preferentially from the matrix when the local strain exceeds a critical value (ref. 16). These broken particles initiate voids, which grow and coalesce resulting in final failure when the critical stress intensity is reached (refs. 29 and 30). Hahn and Rosenfield (ref. 29) experimentally correlated the decrease of toughness with the increased volume fraction of constituents to be of the form:

$$K_{IC} \propto f_c^{-1/6} \tag{5}$$

where

f_c = volume fraction of secondary particles

K_{IC} = fracture toughness.

Limiting the content of Fe and Si, and thus limiting the number of secondary intermetallics has been shown conclusively to increase the fracture toughness of aluminum alloys (refs. 25 and 29). Thus the typical toughness of low impurity 7050-T73 is 35 to 40 MPa $\sqrt{m}$, while that of high impurity 7075-T73 is 25 to 30 MPa $\sqrt{m}$.

There is still some controversy over the effect of dispersoids on fracture toughness in aluminum alloys. Hahn and Rosenfield (ref. 29) contend that dispersoids are more resistant to cracking and are not injurious to toughness. Van Stone and Psioda (ref. 30) disagree with that assessment by pointing out that they have observed formation of void sheets initiated by

dispersoids. Sanders et al. (ref. 17) found that dispersoids affect toughness. Comparing Al_3Zr dispersoids found in 7050 and $Al_{12}Mg_2Cr$ dispersoids present in alloys containing Cr, they found better toughness with the alloy containing Al_3Zr dispersoids. They concluded that the coherent Al_3Zr dispersoids are less effective nucleating sites for microvoids than the corresponding incoherent $Al_{12}Mg_2Cr$ particles found in alloys containing Cr.

There is a general consensus (refs. 21 and 29) that reduction of grain size leads to a better fracture toughness. Sanders and Starke (ref. 21) hypothesized that this is due to more homogenous deformation occurring in small grain size material. However, they also showed that if the small grain size is a result of ITMT treatment, which leads to formation of large intermetallic particles at the recrystallized grain boundaries, a low energy intergranular fracture will occur. Thus the presence of intermetallics is more important than the grain structure.

There is a substantial loss of fracture toughness with increasing yield strength level for the same volume fraction of inclusions (ref. 29). This is attributed to a reduction in the work needed to link the voids in the high strength alloys. Thus the toughness of overaged (T7-type) alloys is greater than that of peak aged (T6-type) alloys.

The fracture toughness of X7091 alloy has not been well established. Otto (ref. 9) reported fracture toughness for X7091 in the T73 temper to be as high as 50 MPa $\sqrt{m}$, which is considerably higher than equivalent 7050 alloy. However, Lyle and Cebulak (ref. 10) found toughness of X7091 alloy to be equal to 7075 but somewhat lower than that of 7050. They attributed the lower fracture toughness in X7091 to a higher content of dispersoids and oxides as compared to 7050.

2.4.3 Stress Corrosion Cracking

Considerable effort has been directed towards determining the causes of SCC. The work has been focused on examination of such microstructural features as PFZ (ref. 31), matrix and grain boundary precipitates (ref. 32), and equalization in electrochemical potentials between the grains and grain boundaries (ref. 33). No clear explanation of the SCC process has emerged and there are great differences in opinion concerning the relative importance of electrochemical and microstructural aspects of the SCC failures. However, the SCC studies have identified several means of improving SCC in aluminum alloys.

A heat treatment was developed which significantly improves the resistance of 7XXX alloys to SCC. This heat treatment, termed T73, consists of aging the alloys to maximum strength (T6), followed by higher temperature aging. The overaging produces a 10 to 20 percent reduction in strength. However, SCC resistance and toughness are improved significantly (ref. 25).

It was also observed that the resistance to SCC increases with increasing copper content. Consequently, alloys containing more copper than 7075 were investigated with the aim of developing both high strength and high resistance to SCC (ref. 34). The product of these studies was the development of the current state of the art I/M alloy 7050. This alloy contains 2.3 percent Cu compared to 1.6 percent Cu for 7075.

The 7XXX P/M alloys have been shown repeatedly to have a better SCC resistance than equivalent I/M alloys (refs. 9, 10, 12, and 21). This was also shown to be the case for the X7091 alloy (refs. 9 and 10). Lyle and Cebulak (ref. 10) postulated that the improvement in SCC resistance for the P/M alloy could be due to a combination of favorable grain morphology, and the presence of Co_2Al_9 dispersoids and oxide particles. They hypothesized that in small grain X7091, the stress corrosion cracks more frequently encountered grain boundaries which were not normal to the tensile stress, and the resolved tensile stress in the boundary under attack dropped. The Co_2Al_9 dispersoids are the most cathodic phase and thus may play an electrochemical role in reducing SCC. Oxides are believed to shift the corrosive attack to a more alkaline condition. Since none of these mechanisms have been conclusively proven to occur, and there is a good probability that other mechanisms might also be involved. More work in this area is needed in order to better understand the factors affecting SCC resistance.

2.5 Crack Initiation and Propagation

The fatigue of metals involves cyclic plastic deformation which is usually strongly influenced by both microstructure and environment. Much effort has been focused on understanding the effects of microstructure and environment on crack initiation and propagation.

2.5.1 Crack Initiation

2.5.1.1 Effects of Slip Character

Crack initiation during cyclic deformation generally occurs in regions where strain has become localized. Strain localization may occur at pre-existing stress concentrations such as notches or corrosion pits, steps produced during fatigue by fretting or by coarse slip offsets at surfaces, and localized regions such as PFZ (ref. 35).

Often, crack initiation is associated with formation of well defined extrusions and intrusions (ref. 36 and 37). Cottrell and Hull (ref. 36) proposed a model (fig. 2) to explain the formation of these features by sequential duplex slip on two intersecting slip bands. Formation of extrusions and intrusions is associated with the presence of slip bands (refs. 38 and 39). Slip bands are an indication that localization of the slip has occurred resulting in localization of the accumulated damage in the slip planes. Since it is easier for slip to occur on the already activated slip planes, slip bands intensify with continuing cycling and result in formation of persistant slip bands (PSB). Due to damage accumulation, cracks ultimately form in the PSB's, multiply and link up to form the fatal crack (ref. 38).

It has been generally recognized that in each stage of fatigue, microstructures that homogenously distribute the strain are desired. However, this is not always the case. The same mechanism may have different effects on various materials. For instance, it has been recognized that inhomogenous planar slip can cause softening in the slip bands, resulting in strain localization (ref. 40). However, as was demonstrated by Saxena and Antolovich (ref. 41) in low stacking fault, Cu-Al alloy planar slip may improve fatigue crack propagation resistance.

In Al-Zn-Mg-Cu alloys the two most important microstructural features which can result in strain localization are shearable precipitates and PFZ (ref. 39). These features can lead to early crack nucleation and enhanced environmental interactions.

2.5.1.2 Coherent Precipitates

Depending on the size and degree of coherency, precipitates are either sheared or looped by dislocations under an applied stress. These interactions are the primary strengthening mechanisms. Subsequent strengthening is reduced when the coherent particles are sheared by dislocations. This results in a local decrease in resistance to dislocation motion, concentration of slip and crack nucleation on slip bands (ref. 39).

As was documented by Papazian et al. (ref. 42), seventy-five percent of the G.P. zones, in the peak aged 7050 alloy, were modified by dislocation interactions when the alloy was fatigue tested in a plastic strain region. Thus localized strains can destroy coherency of the precipitates to an extent where softening occurs (ref. 39).

Overaging reduced the coherency of the precipitates with the matrix and thus reduced strain localization by promoting homogenous slip (ref. 39). Crack nucleation has been shown to be delayed for overaged alloys (ref. 39).

Addition of nonshearable dispersoids intermixed with shearable precipitates has also been shown (ref. 43) to somewhat promote homogenous deformation without the loss of strength which results from overaging.

Sanders and Starke (ref. 21) reported that crack initiation resistance is better with a reduction in grain size for alloys containing shearable precipitates. This was attributed to the reduction of slip length and therefore the stress concentration by reducing the number of dislocations at the grain boundary pile up. The relationship between slip length, number of dislocations at a pile up and stress concentration is as follows (ref. 44):

$$L = \frac{Gnb}{2\sigma_a} \tag{6}$$

where
L = length of dislocation pile up
G = shear modulus
b = Burgers vector
σ_a = applied stress
n = number of dislocations at the pile up

and

$$\sigma = \left(\frac{L}{X}\right)^{1/2} \sigma_a \tag{7}$$

where
σ = stress concentration
x = distance from pile up.

In addition it is generally believed that as grain size is reduced the corresponding deformation changes from nonhomogeneous to homogenous (ref. 39).

2.5.1.3 Precipitate Free Zones

Heterogenous precipitation can occur concurrently with the homogenous precipitation. Nucleation of stable incoherent precipitates occurs preferentially at grain boundaries (ref. 17) and forms solute depleted PFZ adjacent to the boundary. Without the presence of strengthening precipitates, these zones are softer than the matrix and thus lend themselves to localized deformation (ref. 45). The magnitude of stress concentration at PFZ is the function of the grain boundary length, and the difference in strength between the denuded zone and the matrix (ref. 45). Overaging does not homogenize the deformation.

Since the stress concentration is a function of grain boundary length, a reduction in grain size is effective in reducing early crack nucleation (ref. 45). The result can be a change in fracture mode from intergranular to a higher energy transgranular mode.

TMT processing can also reduce the deleterious effects of PFZ on crack initiation (ref. 46). By the introduction of cold work during the processing, step-like ledges can be created at the grain boundaries. This causes reduction in effective slip length within the PFZ and improves the resistance to crack initiation due to lower stress concentration (refs. 39 and 46).

2.5.1.4 Additional Effects on Crack Initiation

In addition to coherent precipitates and PFZ, there are other effects which influence crack initiation. Sanders and Starke (ref. 19) showed the deformation mode in the overaged 7050 alloy may be controlled by the amount of plastic strain. For the samples tested at low plastic strains, formation of inhomogenous dislocation bands was the primary deformation mode. However, at high plastic strains the precipitates were bypassed by a cross-slip mechanism and dislocation cells were formed. When the same alloy was aged to contain only shearable precipitates, deformation mode was unaffected by plastic strain amplitude.

Lin (ref. 47) showed that aggressive environments play an important role in decreasing the resistance to crack initiation. The aggressive H_2O environment decreased the fatigue life of an alloy having shearable precipitates by an order of magnitude in comparison to inert environment for the same plastic strain amplitude.

Sanders and Otto (ref. 11) showed that notched fatigue properties of X7091 alloy were substantially higher than that reported for the 7050 extrusion. They attributed these results to the increased strength and homogeneity of deformation of the P/M alloy. For the same total strain, the higher strength P/M alloy undergoes smaller amounts of plastic strain during each cycle with a resultant increase in total fatigue life before initiation. As mentioned previously, homogenized microstructure reduces stress concentration and inhibits crack nucleation in the P/M alloy.

2.6 Fatigue Crack Propagation

With the realization that most airframe structures contain flaws, the Air Force implemented the damage-tolerant design. The new philosophy (ref. 48)

rejects the unrealistic assumption that no flaws exist, and forces designers to assume that flaws exist in critical structural components. It also places considerably more importance on understanding the factors controlling fatigue crack propagation in metals. Two stages of crack propagation have been recognized and will be discussed in the following sections.

2.6.1 Stage I

This stage is regarded as essentially an extension of the crack nucleation process (ref. 49). In this stage, the crack propagates along crystallographic slip planes {111} with the highest resolved shear stress. Thus, Stage I cracks are usually present on planes oriented 45° to the applied stress. It also has been shown that Stage I cracks often change into Stage II cracks at grain boundaries. Lynch (ref. 35) as well as Nageswararo and Gerold (ref. 49) showed that a Stage I crack propagates by the formation of crystallographic cleavage-like facets. The facets are aligned along the <110> crack propagation direction (ref. 49).

The actual mechanism of Stage I crack propagation is not well understood even though a number of possible mechanisms have been proposed. Laird's (ref. 38) model of Stage I crack propagation is very similar to the various crack initiation models where surface extrusions and intrusions are formed on the slip planes. He suggests that the main difference between the initiation and propagation models is that the screw dislocation carrying PSB strain are distributed equally on all slip planes in case of the initiation model, however, in the Stage I model these screw dislocations are concentrated around the few active slip planes around the notch. By this model, the volume of the crack is exactly balanced by the volume of extrusion.

Lynch (ref. 35) did not find a substantial volume of extrusion in comparison to the volume of the crack. He suggested that intrusions are formed in the slip bands during the tension portion of the cycle. However, noting that Stage I striations are present on the fracture surface, he suggested that the process does not reverse itself during the compressive part of the cycle and instead slip is activated on adjacent slip planes causing deformation behind the crack tip and creating striations which are analogous to Stage II type striations.

Since it has been observed (refs. 35 and 49) that under certain conditions extensive Stage I cracking can occur resulting in a wide range of FCP rates and fracture modes, it is quite possible that more than one mechanism is responsible for Stage I cracking.

2.6.2 Stage II

Transitions from Stage I to Stage II crack growth probably occur when increasing stress intensity or increasing constraint on plastic flow (or both) result in extensive slip on more than one slip plane around crack tip (ref. 35). The transition is accompanied by the change of crack orientation from 45° to ~90° to the stress axis. A more detailed description of microstructural features associated with Stage II crack growth is found further on in this section.

The fatigue crack propagation curves of Stage II crack growth are usually represented on a log-log plot of growth rate (da/dN) versus stress intensity range (ΔK). This plot usually is divided into three separate regions (fig. 3). In region I, for low ΔK, the crack growth rate decreases rapidly with decreasing ΔK and approaches lower limit at ΔK_{th}. Below this threshold (ΔK_{th}) no crack propagation takes place. In region II, midrange of crack growth rates, a power law dependence prevails. In region III, crack growth accelerates as maximum stress intensity (K_{max}) approaches fracture toughness (K_c) (ref. 50).

2.6.2.1 Region I

Relatively little work has been performed in the low growth rate region primarily due to the relatively long testing time and high expense of testing. Recent work on aluminum (ref. 51), iron (ref. 52), and titanium (ref. 53) base alloys suggests that microstructure has a stronger influence of FCG resistance at near threshold ΔK levels than at moderate to high ΔK values.

Bucci et al. (ref. 51) made two interesting observations regarding FCG behavior at low ΔK. 1) The FCG resistance of 7075 and 7050 tends to converge at ΔK below 5.5 Mpa $\sqrt{m}$, whereas at higher ΔK, alloy 7050 is significantly superior to 7075 when tested under constant amplitude loading. 2) A crossover occurs for both alloys at low ΔK, below which peakaged temper (T6) alloys are superior in FCG resistance to overaged (T7) alloys. At intermediate ΔK values the situation is reversed. They hypothesized that since near-threshold crack growth occurs, in part, by slip band decohesion (ref. 54), precipitates represent a major barrier to cyclic slip, and hence crack growth. Thus FCG resistance should deteriorate with increasing interparticle spacing which results from aging. This hypothesis appears to be rather simplistic because it does not take into account the slip mechanism, coherency of particles or the effect of environment.

It is very important to observe that certain microstructural features which might improve resistance to crack initiation, can be detrimental to FCP resistance. For example, as Fine and Ritchie (ref. 55) point out, refining grain size leads to better resistance to crack initiation, however it substantially decreases the resistance to near-threshold crack propagation. The reasons for the decrease in FCG resistance with decreasing grain size have not been well established, even though several models have been suggested.

Lindingkeit et al. (ref. 56) suggested that decrease in grain size created more obstacles for dislocation movement thus decreasing the slip reversibility with decrease in the grain size. The lack of slip reversibility increases dislocation density and increases FCG rates.

Antolovich et al. (ref. 57) noting that deformation structure is similar for both FCP tests (at the crack tip) and LCF tests, tried to explain FCP behavior in terms of cumulative damage type models. They assumed that the cyclic damage accumulation occurs in the process zone, just ahead of the crack tip. Since this process zone would be equal to the grain size for materials exhibiting planar slip, the damage per unit area would be smaller for larger grain size and thus produce slower FCP rates. This model does predict correctly the effect of grain size on FCP. In addition, since Coffin-Manson

exponent β is presented as an inverse of Paris exponent, m, this model also implies that materials with superior LCF behavior, might be inferior in terms of FCP behavior. Further work based on this idea is needed, to qualify the deformation modes for which this model is valid, and to determine the interaction of the deformation structure with the crack itself. This should shed better light on the influence of the deformation structure on fractorgraphic features.

The two above described models are applicable for both Region I and II crack propagation regimes.

Fine and Ritchie (ref. 55) also point out that environment plays an important part on near threshold propagation. Testing in vacuum resulted in substantially slower crack growth rates in steel, titanium and aluminum alloys as compared to tests performed in ambient atmosphere.

In most alloys the fracture morphology characteristic of low ΔK regime is in the form of crystallographic transgranular or intergranular facets (ref. 55). In the case of 7XXX alloys tested in high humidity environment, the fracture characteristics are typified by the presence of crystallographic cleavage facets as well as the presence of noncrystallographic flat and featureless plateaus (ref. 51). Striations are usually not present in the low ΔK regime.

2.6.2.2 Region II

At the intermediate crack growth rates the crack propagation rate has been found to follow a power law relationship. This relationship was developed by Paris and Erdogan (ref. 58) and shows the dependence of crack growth rate on the applied stress intensity range (ΔK)

$$\frac{da}{dN} = R(\Delta K)^m \qquad (8)$$

where
R,m material constants.
This relationship accurately describes FCP data for many materials at the intermediate ΔK level.

In this intermediate stress intensity range region, Stage II crack growth usually prevails and is accompanied by the formation of surface striations (ref. 59). Striations represent the propagation distance of a fatigue crack during each stress cycle (ref. 38).

Numerous models have been proposed to account for the mechanism of striation formation during FCP. The two most prominent models are that of Laird (ref. 60) and Tomkins and Biggs (ref. 61). Laird's model is known as the "plastic-blunting process" (fig. 4). This model basically consists of plastic-blunting/alternate shear process at crack tip during unloading by slip behind the crack tip. The Tomkins-Biggs model (fig. 5) involves "sliding off" of material in flow bands at the crack tip which is controlled by strain hardening.

Environment has been shown to influence both FCP rate (refs. 17, 35, and 62 through 64) and fracture topography (refs. 1, 35, and 62) in aluminum alloys tested in the intermediate crack growth rate regime. Some of the general conclusions obtained from these studies are listed below:

1. Resistance of alloys 7050 and 7X75 in comparable tempers to FCP is similar in dry environment. However, in ambient and moist atmospheres or in aqueous and salt environments, intermediate FCG rates of alloy 7050 are generally slower than those of 7X75-type alloys of comparable temper (ref. 17 and 64).

2. Overaging 7XXX alloys from the peak strength T6 temper to T7-type tempers increases resistance to FCG in the presence of moisture (refs. 17, 63, and 64).

3. Increasing copper content in 7XXX alloys reduces constant amplitude fatigue crack growth rates in the presence of moisture (refs. 17 and 64).

The variables which increases alloys resistance to SCC (i.e., overaging, Cu content) also increase the resistance to FCG in the intermediate stress intensity range. However, it is also important to notice that even in the T73 temper, which is resistant to standard SCC tests, the FCP in aqueous environment is faster than that in ambient environment (ref. 63).

It should be noted that the influence of the microstructure is not the same at intermediate ΔK, as it is at low ΔK. While aging from T6 to T7 temper reduces FCP rates by a factor of two at intermediate ΔK, it increases FCG rates up to ten times at low ΔK (ref. 51).

The fracture topography is very dependent on environment in the intermediate crack growth rates regime. In the inert environment the fracture surface is noncrystallographic and essentially striation free (refs. 35 and 39). With the presence of aggressive environments such as water vapor or liquid metal, the fracture surface becomes highly crystallographic (refs. 35, 50, and 62). The fracture takes place on the cleavage planes on which striations can easily be identified (refs. 35, 50, and 62). The identification of the cleavage planes on which fracture occurs has been controversial. The cleavage planes have been identified as either {111} (ref. 65), {100} (ref. 35) or {110} (ref. 62). Hertzberg (ref. 50) indicated that fracture on {100} planes and <110> direction is in the agreement with theoretical considerations. A detailed evaluation by Lynch (ref. 35) showed that the striations tended to form on {111} slip planes parallel to <110> direction. This resulted in a macroscopical crack propagation on {100} cleavage planes in the <110> direction.

As the environment becomes progressively more aggressive, a corresponding change in the topography of striations takes place. The profile of striations changes from well developed "ductile" striations to less developed "brittle" striations with more aggressive environments (refs. 35, 62, and 65).

Various mechanisms such as adsorption (ref. 66), chemisorption (ref. 35) and hydrogen embrittlement (ref. 62) have been proposed as the cause of embrittling the fracture surface and increasing FCP rates. Lynch (ref. 35) argues persuasively that ductile striations are formed when extensive slip at

the crack tip is possible. Limitations in operative slip systems result in "brittle" striations. He further argues that chemisorption limits three of the five slip systems from being operative thus resulting in the presence of "brittle" striations. Corroborating evidence that only a limited number of slip systems are operative in an aggressive environment is contained in the observations (refs. 35 and 49) that the plastic zone size is both reduced and localized in the aggressive environments.

In the case of 7XXX I/M alloys no significant effect of constituent particles, dispersoids or other microstructural features was observed in the intermediate ΔK region for constant amplitude testing (refs. 17 and 64).

At intermediate crack growth rates the FCP resistance of X7091 alloy has been shown to be inferior to that of comparable I/M alloys (refs. 10 to 12). Sanders and Otto (ref. 11), noting that the fracture topography of X7091 was smoother and less tortuous than that of comparable 7050 alloy, attributed the inferior FCP behavior of X7091 to its finer and more homogenous microstructure, which offered nothing to divert the crack from its macroscopic growth direction. In 7050, second phase particles and nonhomogenous grain structure lead to crack diversion and slower FCG rates. The extent to which this change in topography affects FCG rates has not been quantified, and therefore this phenomenon may only be of a secondary importance.

Sanders and Otto (ref. 11) further argue that to understand the FCG results, the size of the plastic zone (r_p) and its relation to the size and spacing of pertinent microstructural features should be considered. If the size of r_p is significantly greater than given microstructural feature, then that feature should have relatively little effect on FCG rate, since the microstructure behaves as a continuum. By using this hypothesis they tried to explain superior FCP behavior of 7050 at low ΔK regime. However, this does not explain the superior 7050 behavior in the intermediate ΔK regime, where their own calculations show that both alloys should act as a continuum according to the hypothesis. Also, considering that resistance to SCC plays a very important role in determining the FCG behavior at intermediate ΔK, and that X7091 has been shown to have superior SCC resistance (refs. 10, 12, 21, and 22), it is puzzling why FCP of X7091 is inferior to that of 7050.

It is also worthwhile to point out again that microstructural features which lead to a better resistance to crack initiation, may be detrimental towards crack propagation. X7091 alloy shows superior resistance to crack initiation (ref. 11) and yet the same microstructure leads to inferior FCP behavior.

2.6.2.3 Region III

The crack propagation at high ΔK is not as important as it is for the other two regions because the proportion of the total life spend in the region is miniscule in the comparison with regions I and II.

Region III is characterized by acceleration of crack growth resulting from local fracture as K_{max} approaches toughness, K_c (ref. 50). Since fracture toughness plays an important role in determining FCP rates at high ΔK, it can be expected that the microstructural features which lead to high toughness, will also result in superior FCP behavior at high ΔK.

Sanders and Staley (ref. 16) showed that fracture surface at high ΔK had a considerably higher percentage of constituent particles than a randomly cut plane through the specimen. The fracture surface at lower ΔK revealed approximately the same percentage of constituents as the randomly cut plane. Consequently, the brittle constituents provide preferential crack path ahead of the crack tip at higher stress intensities.

The typical fracture surface at high ΔK is similar in appearance to monotonic failure and consists of separation between large intermetallic particles and the matrix. Cracks are formed, which join by coalescence of voids (ref. 16).

2.7 Load History

In airframe structures, the load history typically encountered is of variable amplitude (also known as spectrum loading) rather than constant amplitude loading. Variable amplitude loading resulting from aircraft maneuvers or severe gusts can affect crack growth and life predictions considerably. Research in the last two decades (refs. 16, 63, and 67 through 76) has shown that load sequences have a considerable effect on FCP rates. Most of the work was focused on understanding the effect of single and block overloads and underloads on FCG rates (refs. 17, 63, and 67 to 72). The basic findings of these studies are summarized below:

1. Positive overloads introduce significant crack growth delays. In general, longer delays are obtained by increasing the magnitude of the overload and application of blocks of overloads instead of single overloads.

2. The retardation need not immediately follow the overloads, further growth may occur before retardation.

3. Negative overloads have a relatively small detrimental effect on crack growth. However, a negative overload added immediately after positive overload can significantly reduce crack growth retardation. Thus there is an apparent sequence effect.

4. Hi-lo load sequence (number of high loads followed by smaller loads) has similar results as overload cycles. Lo-hi sequence interaction effects are hardly detectable.

5. In general, a lower yield strength alloy will produce longer delays than high strength alloy.

6. Aggressive environment acts to reduce the crack growth retardation.

7. The number of delay cycles decreases with an increase of thickness (i.e., change from stress to plane strain).

2.7.1 Variable Amplitude Loading Prediction Models

Two types of models have been developed to account for the crack growth delay following overloads. Plastic zone size models developed by Willenborg (ref. 77) and Wheeler (ref. 78) account for the retardation following an overload by the presence of residual stresses in the crack tip plastic zone.

Thus, in the Willenborg model the residual stress has to be subtracted from the applied stress in order to obtain the lower effective stress intensity (ΔK_{eff}) which results in lower FCG rates. The ΔK_{eff} is then inputed into the Paris equation to predict the FCG rate. Neither Wheeler's nor Willenborg's models account for the effect of negative stresses. The model by Wozumi et al. (ref. 79), also based on the plastic zone size considerations, makes an attempt to account for the negative overloads.

The plastic zone size-type models fail to account for two experimentally observed phenomena: (1) delay in crack growth retardation after an overload, and (2) increase in retardation with the number of applied high load cycles (ref. 72).

The other class of models which have gained increasingly wider recognition and acceptance are the crack closure models (refs. 80 through 82). These models, first postulated by Elber (ref. 80), show that a crack remains closed for a portion of the load cycle after an overload is applied. They predict the observed delayed retardation by pointing out that retardation only takes place when the crack penetrates the plastic zone created by the overload. These models also predict an increase of retardation with the number of applied overloads. A ΔK_{eff} is calculated by subtracting the stress intensity needed to open the crack from the applied stress intensity. As in Willenborg's model, the ΔK_{eff} is then fed into the Paris equation to obtain FCG rate predictions. Both overloads and underloads are accounted for in the crack closure models.

The crack closure models have become increasingly more sophisticated and complex. For example, Dill and Saff (ref. 81) developed a model based on the potential interference of the crack surfaces. The potential interference is treated as a wedge acting behind the crack tip and the contact stresses created by this wedge are computed through an elastic plastic analysis. Due to high complexity of the calculations, extensive and expensive computer usage is required to perform the analysis.

A more quantitative description of both the plastic zone size and crack closure models is provided in appendix A.

In order to simulate crack growth under more realistic loading history conditions, more emphasis has been placed recently upon the evaluation of fatigue crack growth under complex spectra (refs. 73 through 76, and 83).

Since these complex spectra contain usually thousands of load points, it is very important to understand the load interactions. Dill et al. (ref. 75) and Albekis (ref. 76) examined numerous variations of the base line spectra to determine their effect on spectrum FCG rates. Dill et al. (ref. 75) found that the greatest effect on FCP was the addition (or removal) of the highest peak load. Truncations of cycles below that of 45 percent of the maximum had no significant effect of FCG rate. Truncations of cycles at higher levels, significantly decreased FCG rates. Elimination of compressive loads only slightly decreased the FCG rates. Albekis (ref. 76) observed similar effects occurring. The spectrum results were analyzed by the use of both plastic zone size and crack closure models. The analysis revealed that no single model was able to predict crack growth for all the spectrum variations. Thus various aspects of load interaction phenomena lack satisfactory explanations.

Retardation phenomena, using even a simple spectrum are complex, and must be systematically investigated before a reliable procedure for predicting fatigue lives under actual spectra can be developed.

The major weakness of all these models is that they do not take into account either metallurgical or environmental factors. For instance, Willenborg's model (ref. 77) predicts that materials with the same yield strength will exhibit similar retardation behavior. Chanani (ref. 63) found that this was not the case for 2024-T8 and 7050-T73 heat treated to the same yield strength. He concluded that metallurgical variables such as precipitate morphology, dislocation interactions, and cyclic hardening have to be taken into account to explain the disparity in crack growth rates.

2.7.2 Constant Amplitude Versus Spectrum FCG Behavior

Ranking of aluminum alloys with respect to FCG resistance under both simple and complex spectrum loading is not always the same as the ranking achieved under constant amplitude loading. Comparison between spectrum and constant amplitude loading is difficult, due to the fact that it is troublesome to pinpoint the equivalent stress intensities for which a comparison of FCG rates can be established. However, a study (ref. 83) of seven 2XXX and 7XXX alloys exposed to both complex spectra (two highly different spectra) and constant amplitude loading, at various stress intensities, revealed that even though some similarities in ranking were observed, in general the rankings could not be correlated at any stress intensity. Interestingly, the rankings of these seven alloys were the same when compared for the two very different load spectra utilized in the program.

Sanders et al. (ref. 17) showed that even though the FCG resistance of 7050 is better than that of 7075 under constant amplitude loading, under simple spectrum loading the ranking of the alloys changed. They attributed the better spectrum FCG resistance of 7075 to large amount of secondary cracking in the front of the crack tip which in turn reduced the applied stress intensity and thus reduced the FCG. The secondary cracking originated at the brittle constituent particles thus pointing out that a microstructural feature thought to be detrimental to FCG resistance, may in some cases actually improve FCG resistance.

It is clear that FCG under constant amplitude and especially under spectrum loading is a very complex phenomenon to analyze. Different competing mechanisms, whether they may be related to microstructural, environmental or load history effects, have to be considered. However, a large amount of good research, especially in the area of constant amplitude loading, provides a good foundation required to pursue an understanding of the FCG under spectrum loading.

3. Conclusions

Literature survey was conducted to determine the effects of different microstructural features and different load histories on monotonic and cyclic properties of aluminum alloys. Comparison of microstructure between P/M and I/M alloys was made. The two alloys on which the comparison is focused are X7091 and 7050. Based on the survey the following conclusions are made:

1. Alloys produced by rapidly solidified P/M process exhibit fine grain structure, dispersoid and fine oxide particles, and very few brittle intermetallic inclusions. The slowly solidified I/M alloys possess grain size on the order of magnitude larger than P/M alloys, dispersoid particles and large brittle intermetallic inclusions. The strengthening precipitates present in both type of alloys are similar and depend on the aging treatment.

2. P/M alloys exhibit 5 to 10 percent higher strength than the corresponding I/M alloys. The lack of pronounced Hall-Petch effect in P/M alloys has been attributed to the dominance of strengthening precipitates.

3 Fracture toughness is inversely proportional to the volume fracture of brittle inclusions. Small grain size also has been suggested to improve toughness by the presence of homogenous slip, which reduces stress concentrations.

4. P/M alloys have a better resistance to SCC than comparable I/M alloys. Several mechanisms have been proposed to explain this behavior, however none have been proven.

5. Crack initiation is enhanced by localization of strain. Thus, small grain size, which reduces inhomogeneous slip, increases crack initiation resistance. Overaging or addition of nonshearable dispersoids improves crack initiation resistance by also promoting homogenous slip. Decrease in PFZ also improves crack initiation resistance.

6. Two stages of fatigue crack growth have been recognized. In stage I, cracks propagate along crystallographic slip planes, with the cracks being approximately 45° to the applied stress direction. Stage II cracks propagate by striation forming mechanism and are approximately 90° to the applied stress.

7. FCG rates are increased by a reduction in grain size thus P/M alloys show inferior FCG behavior. Aggressive environments increase FCG rates. Various mechanisms such as adsorption, chemisorption and hydrogen embrittlement have been proposed to account for influence of environment of FCG behavior.

8. Load sequence, environment and thickness have a considerable effect on FCG behavior of a given alloy.

9. The two main types of models used to predict spectrum FCG behavior are crack closure and plastic zone size models. No single model was able to satisfactorily predict FCG rates for all load histories. It is suggested that microstructural features have to be taken into account in order to fully explain FCG behavior.

APPENDIX A

This appendix contains definition and discussion of two retardation models.

1) Willenborg Model

Since the rate of propagation of a fatigue crack is controlled by the stress intensity factor at the crack tip, the magnitude of the stress intensity factor is a good indication of extent of crack tip deformation. Willenborg et al. (ref. 77) proposed an "effective stress" concept which may differ form the applied stress and thus change the applied stress intensity.

Willenborg Nomenclature:

R_p = plastic-zone size due to overload cycle
R_e = remaining distance across plastic zone after a period of cyclic growth rate
R_y = calculated plastic zone size for the next load

An accepted expression for plastic zone is

$$R_p = \frac{K^2}{N^2 n \sigma y^2} \tag{A1}$$

where N_R varies from 1 for plane stress to 3 for plane strain. After a period of cyclic crack growth:

$$R_e = \frac{K_{req}^2}{N_R n \sigma_y} \tag{A2}$$

where K_{req} is the stress intensity required to reach the previous plastic zone boundary.

If R_y for the next load is less than R_e, the stress intensity should be reduced by the amount it falls short of reaching R_E.

$$K_{eff} = K_{next} - (K_{req} - K_{next}) = 2K_{next} - K_{req} \tag{A3}$$

Solving for K_{req} from (A2) and substituting to (A3) leads to:

$$K_{eff} = 2K_{next} - \sigma_p \sqrt{R_e \times N_R} \cdot n \tag{A4}$$

The Willenborg model states that any load causing a plastic zone less than 50 percent of the load required to extend the plastic zone will have no crack-growth. For loads between 50 percent and 100 percent of that required to extend the plastic zone, retardation varies from fully arrested at 50 percent to fully unretarded at 100 percent.

2) Generalized Crack Closure Model

Elber (ref. 80) observed that the surface of the fatigue crack closed during FCP tests under cyclic tension loading. Based on these observations, he suggested that the tip of a fatigue crack closes while specimens were still subject to a tension load, and that the crack propagates only during that portion of the load cycle in which it is fully open. Thus the effective stress range, $\Delta\sigma_{eff}$ is:

$$\Delta\sigma_{eff} = \sigma_{max} - \sigma_o \tag{A5}$$

where σ_{max} is the maximum mum applied load and σ_o is the crack opening load. Also,

$$\Delta\sigma_{eff} = \sigma_{max} (1 - C_f) \tag{A6}$$

where C_f is the closure factor defined as

$$C_f = \frac{\sigma_o}{\sigma_{max}} \tag{A7}$$

Bell et al. (ref. 82) use the Elber crack closure to modify the Paris equation as:

$$\frac{da}{dN} = \left[R \frac{\sigma_{max} - \sigma_o}{(1 - C_{f_o})} \sqrt{\pi a} \right]^m \tag{A8}$$

for the case of through crack in an infinite sheet. The coefficients R and m are determined by Paris equation. C_{f_o} is the closure factor at R = 0, and is the half crack length.

REFERENCES

1. Staley, J. T.: Aluminum Alloy and Process Developments for Aerospace. Met. Eng. Q., vol. 16, May 1976, pp. 52-57.

2. Staley, J. T.; and Hunsicker, H. Y.: Exploratory Development of High Strength, Stress-Corrosion Resistant Aluminum Alloy for Use in Thick Section Applications. AFML-TR-70-256, Wright-Patterson AFB, 1970. (AD-877677)

3. Thompson, D. S.; Subramanya, B. S.; and Levy S. A.: Quench Rate Effects in Al-Zn-Mg-Cu Alloys. Metall. Trans. vol. 2, Apr. 1971, pp. 1149-1160.

4. Roberts, S. G.: Powder Fabrication of Aluminum Alloys. ASD-TR-56-481, Kaiser Aluminum and Chemical Corp., 1957. (AD-090525)

5. Roberts, S. G.: Research Study for Development of Aluminum Base Alloys by Powder Metallurgy Techniques. MSPR 61-69, Kaiser Aluminum and Chemical Corp., Nov. 1961.

6. Towner, R. J.: Development of Aluminum-Base Alloys. Rept. 7-62-AP59-8, Aluminum Co. of America, Sept. 1962.

7. Haarr, A. P.: Development of Aluminum Base Alloys -- Section III. FR-13-65-AP59-S, Aluminum Co. of America, May 1966.

8. Cevulak, W. S.: Program to Develop High Strength Aluminum Powder Metallurgy Products. Phase IVA: Vacuum Process Verification. Quarterly Report, Sept. 20-Dec. 20, 1972. Aluminum Co. of America, 1973. (AD-908435L)

9. Otto, W. L., Jr.: Metallurgical Factors Controlling Structure in High Strength P/M Products, AFML-TR-76-60, Wright-Patterson AFB, May 1976.

10. Lyle, J. P.; and Cebulak, W. S.: Powder Metallurgy Approach for Control of Microstructure and Properties in High Strength Aluminum Alloys. Metall. Trans., vol. 6A, Apr. 1975, pp. 685-699.

11. Sanders, R. E.; and Otto, W. L.: The Fatigue Resistance of High Strength 7XXX P/M Aluminum Alloy Extrusions. Prog. Powder Metall., vol. 35, 1980.

12. Lawley, A.; and Koczak, M. J.: A Fundamental Study of Fatigue in Powder Metallurgy Aluminum Alloys. Drexel Univ., Aug. 1981. (AF-AFOSR-3247-77, AD-A105080)

13. Mondolfo, L. F.; Gjostein, N. A.; and Levinson, D. W.: Structural Changes During the Aging in an Al-Mg-Zn Alloy. Trans. Am. Inst. Min. Eng. vol. 206, 1956, pp. 1378-1385.

14. Lyman, C. E.; and VanderSande, J. B.: A Transmission Electron Microscopy Investigation of the Early Stages of Precipitation in an Al-Zn-Mg Alloy. Metall. Trans., vol. 7A, Aug. 1976, pp. 1211-1216.

15. Hornbogen, E.: Nucleation of Precipitates in Defect Solid Solutions. Nucleation, A. C. Zettlemoyer, ed., Marcel Dekker, 1969, pp. 309-378.

16. Sanders, T. H., Jr.; and Staley, J. T.: Review of Fatigue and Fracture Research on High-Strength Aluminum Alloys. Fatigue and Microstructure, American Society for Metals, 1979, pp. 467-522.

17. Sanders, T. H., Jr.; et al.: Effect of Microstructure on Fatigue Check Growth of 7XXX Aluminum Alloys Under Constant Amplitude and Spectrum Loading. Rept-56-78-AF8, Aluminum Co. of America, Apr. 1978.

18. Smith, W. F.; Grant, N. J.: Mechanism of Formation of Precipitate-Free Zones in an Al-4.7 percent Zn-3.9 percent Mg Alloy. Trans. Am. Soc. Met., vol. 62, no. 3, Sept. 1969, pp. 724-728.

19. Sanders, T. H., Jr.; and Starke, E. A., Jr.: The Relationship of Microstructure to Monotonic and Cyclic Straining of Two Age Hardening Aluminum Alloys. Metall. Trans., vol. 6A, Sept. 1876, pp. 1407-1418.

20. Clark, J. B., Jr.: Electron Probe Test of Two Theories of Denuded Zone Formation in Aged Alloys. Acta. Metall., vol. 12, no. 10, 1964, pp. 1197-1201.

21. Sanders, R. E.; and Starke, E. A.: The Effect of Intermediate Thermomechanical Treatments on the Fatigue Properties of a 7050 Aluminum Alloy. Metall. Trans., vol. 9A, Aug. 1978, pp. 1087-1100.

22. Pelloux, R. M. N.: Fractographic Analysis of the Influence of Constituent Particles on Fatigue Crack Propagation in Aluminum Alloys. Trans. Am. Sci. Met., vol. 57, 1964, pp. 511-518.

23. Mondolfo, L. F.: Structure of the Aluminum-Magnesium-Zinc Alloys. Metall. Rev., vol. 16, no. 153, June 1971, pp. 95-124.

24. Skinner, D. J.; et al.: The Aging Response of a High Strength P/M Aluminum Alloy. Mod. Dev. Powder Metall., vol. 13, 1981, pp. 483-499.

25. Starke, E. A.: Aluminum Alloys of the 70's; Scientific Solutions to Engineering Problems. Mater. Sci. Eng., vol. 29, 1977, pp. 99-115.

26. Orowan, E.: Discussion, Session III - Effects Associated with Internal Stresses. Symposium on Internal Stresses in Metals and Alloys, Institute of Metals (London), 1948, pp. 451-453.

27. Ludtka, G. M.; and Laughlin, D. E.: The Effect of Solute Content on the Slip Behavior in 7XXX Series Aluminum Alloys. Metall. Trans., vol. 12A, Dec. 1981, pp. 2083-2091.

28. Thompson, D. S.; and Zinkham, R. E.: Program to Improve the Fracture Toughness and Fatigue Resistance of Aluminum Sheet and Plate for Aircraft Applications, vol. 2. AFML-TR-73-247, vol.-II, Reynolds Metals Co., 1974. (AD-A003417)

29. Hahn, G. T.; and Rosenfield, A. R.: Metallurgical Factors Affecting Fracture Toughness of Aluminum Alloys. Metall. Trans., vol. 6A, Apr. 1975, pp. 653-668.

30. VanStone, R. H.; and Psioda, J. A.: Discussion of Metallurgical Factors Affecting Fracture Toughness of Aluminum Alloys. Metall. Trans., vol. 6A, Apr. 1975, pp. 668-670.

31. Adler, P.; DeIasi, R.; and Geschwind, G.: Influence of Microstructure on the Mechanical Properties and Stress Corrosion Susceptibility of 7075 Aluminum Alloy. Metall. Trans., vol. 3, Dec. 1972, pp. 3191-3200.

32. Jacobs, A. J.: The Mechanism of Stress Corrosion Cracking in 7075 Aluminum. Fundamental Aspects of Stress Corrosion Cracking. National Assoc. of Corrosion Engineers, 1969, pp. 530-560.

33. Sprowls, D. O.; and Brown, R. H.: Stress Corrosion Mechanisms for Aluminum Alloys. Fundamental Aspects of Stress Corrosion Cracking. National Assoc. of Corrosion Engineers, 1969, pp. 466-506.

34. Staley, J. T., Hunsicker, H. Y.; and Schmidt, R.: New Aluminum Alloy X7050, TMS Paper F-71-7, 1971.

35. Lynch, S. P.: Mechanisms of Fatigue and Environmentally Assisted Fatigue. Am Soc. Test. Mater. Spec. Tech. Publ. 675, 1979, pp. 174-213.

36. Cottrell, A. H.; and Hull, D.: Extrusion and Intrusion by Cyclic Slip in Copper.. Proc. R. Soc. London, vol. A242, Nov. 19, 1957, pp. 211-213.

37. Boettner, R. C.; and McEvily, A. J., Jr.: Fatigue Slip Band Formation in Silicon-Iron. Acta. Metall., vol. 13, Sept. 1965, pp. 937-946.

38. Laird, C.: Mechanisms and Theories of Fatigue. Fatigue and Microstructure, Amer. Society for Metals, 1979, pp. 149-203.

39. Starke, E. A.; and Lutjering, G.: Cyclic Plastic Deformation and Microstructure. Fatigue and Microstructure, Amer. Society for Metals, 1979, pp. 205-243.

40. Calabrese, C.; and Laird, C.: Mater. Sci. Eng. vol. 13, 1974, pp. 141-157.

41. Saxena, A.; and Antolovich, S. D.: Low Cycle Fatigue, Fatigue Crack Propagation and Substructures in a Series of Polycrystalline Cu-Al Alloys. Metall. Trans., vol. 6A, Sept. 1975, pp. 1809-1828.

42. Papazian, J. M.; Deiasi, R. J.; and Adler, P. N.: A Calorimetric Study of Fatigue Induced Microstructural Changes in Aluminum Alloy 7050, Metall. Trans., vol. 11A, Jan. 1980, pp. 135-140.

43. Lutjering, G.; Doker, H.; and Munz, D.: Microstructure and Fatigue Behavior of Al-Alloys. Microstructure and Design of Alloys, Institute of Metals (London), 1973, pp. 427-431.

44. Weertman, J.; and Weertman, J. R.: Elementary Dislocation Theory. Macmillan, 1964, pp. 128-130.

45. Carlson, M. F.; and Ritchie, R. O.: On the Effect of Prior Austenite Grain Size on Near-Threshold Fatigue Crack Growth. Sci. Metall., vol. 11, 1977, pp. 1113-1118.

46. Welpmann, K.; Lutjering, G.; and Bunk, W.: Influence of TMT on Fracture Properties of Aluminum Alloys. Proceedings of the 4th int. Conf. on Fracture, D. M. R. Taplin, ed., Univ. of Waterloo Press, vol. 2, 1977, pp. 105-110.

47. Lin, F. S.: Low Cycle Corrosion Fatigue and Corrosion Fatigue Crack Propagation of High-Strength-1000-Type Aluminum Alloys. Ph.D. Thesis, Georgia Institute of Technology, 1978.

48. Aircraft Structural Integrity Program. Airplane Requirements. MIL-Std 1530A, Dept. of Defense, Dec. 1975.

49. Nageswararo, M.; and Gerold, V.: Fatigue Crack Propagation in Stage I in an Aluminum-Zinc-Magnesium Alloy: General Characteristics, Metall. Trans., vol. 7A, Dec. 1976, pp. 1847-1855.

50. Hertzberg, R. W.: Deformation and Fracture Mechanics of Engineering Materials. J. W. Wiley, 1976, pp. 486.

51. Bucci, R. J.; et al.: Effect of Microstructure on 7XXX Aluminum Alloy FCG at Low Stress Intensities, Aluminum Co. of America, Oct. 1980.

52. Ritchie, R. O.: Influence of Microstructure on Near-Threshold Fatigue-Crack Propagation in Ultra-High Strength Steels. Met. Sci., vol. 11, Aug.-Sept. 1977, pp. 368-381.

53. Yoder, G. R.; Cooley, L. A.; and Crooker, T. W.: Enhancement of Fatigue Crack Growth and Fracture Resistance in Ti-6Al-4V and Ti-6Al-6V-2Sn Through Microstructural Modification. J. Eng. Mater. Technol., vol. 99, no. 4, Oct. 1977, pp. 313-318.

54. Hertzberg, R. W.; and Mills, W. J.: Character of Fatigue Fracture Surface Micromorphology in the Ultra-Low Growth Rate Regime. Am. Soc. Test. Mater. Spec. Tech. Publ. 600, 1976, pp. 220-234.

55. Fine, M. E.; and Ritchie, R. O.: Fatigue-Crack Initiation and Near-Threshold Crack Growth. Fatigue and Microstructure, American Society for Metals, 1979, pp. 245-278.

56. Lindigkeit, J.; et al.: The Effect of Grain Size on the Fatigue Crack Propagation Behavior of Age-Hardened Alloys in Inert and Corrosive Environment. Acta. Metall., vol. 27, Nov. 1979, pp. 1717-1726.

57. Antolovich, S. D.; Saxena, A.; and Chanani, G. R.: A Model for Fatigue Crack Propagation. Eng. Fract. Mech., vol. 7, no. 4, 1975, pp. 649-652.

58. Paris, P. C.; and Erdogan, F.: A Critical Analysis of Crack Propagation Laws. J. Basic Eng., vol. 85, Dec. 1963, pp. 528-534.

59. Ermi, A. M.: Correlation of Substructure and Crack Behavior with Creep-Fatigue Properties of 304 Stainless Steel. Ph.,D. Thesis, U. of Cincinnati, 1979.

60. Laird, C.: The Influence of Metallurgical Structure on the Mechanisms of Fatigue Crack Propagation. Fatigue Crack Propagation, Am Soc. Test. Mater. Spec. Tech. Publ. 415, 1967, pp. 131-168.

61. Tomkins, B.; and Biggs, W. D.: Low Endurance Fatigue in Metals and Polymer, Pt. 3. Mechanisms of Failure. J. Mater. Sci., vol. 4, 1969, pp. 544-553.

62. Nix, K. J.; and Flower, H. M.: The Micromechanisms of Fatigue Crack Growth in a Commercial Al-Zn-Mg-Cu Alloy. Acta. Metall., vol. 30, Aug. 1982, pp. 1549-1559.

63. Chanani, G. R.: Fundamental Investigation of Fatigue Crack Growth Retardation in Aluminum Alloys. AFML-TR-76-156, Northrup Corp., 1976. (AD-A037184)

64. Truckner, W. G.; et al.: Effect of Microstructure on Fatigue Crack Growth of High-Strength Aluminum Alloys, AFML-TR-76-169, Aluminum Co. of America, 1976. (AD-A037156)

65. Thompson, K. R. L.; and Craig, J. V.: Fatigue Crack Growth Along Cleavage Planes in an Aluminum Alloy. Metall. Trans., vol. 1, Apr. 1970, pp. 1047-1049.

66. Deveraux, O. F.; McEvily, A. J.; and Staehle, R. W.: Corrosion Fatigue: Chemistry, Mechanics and Microstructure. National Association of Corrosion Engineers, 1972.

67. Bucci, R. J.; et al.: Ranking 7XXX Aluminum Alloy Fatigue Crack Growth Resistance Under Constant Amplitude and Spectrum Loading. Am. Soc. Test. Mater. Spec. Tech. Publ. 714, 1980, pp. 41-78.

68. Bucci, R. J.: Spectrum Loading - A Useful Tool to Screen Effects of Microstructure on Fatigue Crack-Growth Resistance. Am. Soc. Test. Mater. Spec. Tech. Publ. 631, 1977, pp. 388-401.

69. Jonas, O.; and Wei, R. P.: An Exploratory Study of Delay in Fatigue-Crack Growth. Int. J. Fract. Mech., vol. 7, Mar. 1971, 116-118.

70. Schijve, J. J.: Effect of Load Sequences on Crack Propagation Under Random and Program Loading. Eng. Fract. Mech., vol. 5, June 1973, pp. 269-280.

71. Stephens, R. I.; Chen, D. K.; and Hom, B. W.: Fatigue Crack Growth with Negative Stress Ratio Following Single Overloads in 2024-T3 and 7075-T6 Aluminum Alloys. Am. Soc. Test. Mater. Spec. Tech. Publ. 595, 1976, pp. 27-40.

72. Alzos, W. X.; Skat, A. C., Jr.; and Hillberry, B. M.: Effect of Single Overload/Underload Cycles on Fatigue Crack Propagation-in Al Alloys. Am. Soc. Test. Mater. Spec. Tech. Publ. 595, 1976, pp. 41-58.

73. Schijve, J.: Observations on the Prediction of Fatigue Crack Growth Propagation Under Variable-Amplitude Loading. Am. Soc. Test. Mater. Spec. Tech. Publ. 595, 1976, pp. 3-23.

74. Wanhill, R. J. H.: Maneuvre Spectrum Fatigue Crack Propagation in Aluminum Alloy Sheet Materials. NLR-TR-78091-U, National Aerospace Lab (Amsterdam, Netherlands), 1980.

75. Dill, H. D.; Saff, C. R.; and Potter, J. M.: Effects of Fighter Attack Spectrum on Crack Growth. Am. Soc. Test. Mater. Spec. Publ. 714, 1980, pp. 205-217.

76. Abelkis, P. R.: Effect of Transport Aircraft Wing Loads Spectrum Variation on Crack Growth. Am. Soc. Test. Mater. Spec. Publ. 714, 1980, pp. 143-169.

77. Willenborg, J.; Engle, R. M.; and Wood, H. A.: A Crack Growth Retardation Model Using an Effective Stress Concept. TM-7-1-FBR, Air Force Flight Dynamics Lab., 1971.

78. Wheeler, O. E.: Spectrum Loading and Crack Growth. J. Basic Eng., vol. 94, no. 1, Mar. 1972, pp. 181.

79. Wozumi, J. T.; Spamer, T.; and Lambert, G. E.: An Engineering Model for Assessing Load Sequencing Effects. Am. Soc. Test. Mater. Spec. Publ. 714, 1980, pp. 128-142.

80. Elber, W.: the Significance of Fatigue Crack Closure. Am. Soc. Test. Mater. Spec. Publ. 486, 1971, pp. 230-242.

81. Dill, H. D.; and Saff, C. R.: Effect of Fighter Attack Spectrum on Crack Growth. AFFDL-TR-76-112, Wright-Patterson Air Force Base, 1977. (AD-A042369)

82. Bell, P. D.; and Creager, M.: Crack Growth Analysis for Arbitrary Spectrum Loading. AFFDL-TR-74-129, Grumman Aerospace Corp., 1974. (AD-A021700)

83. Chanani, G. R.: Methodology for Evaluation of Fatigue Crack Growth Resistance of Aluminum Alloys under Spectrum Loading. NOR-82-54, Northrop Corp., 1982. (AD-A116500)

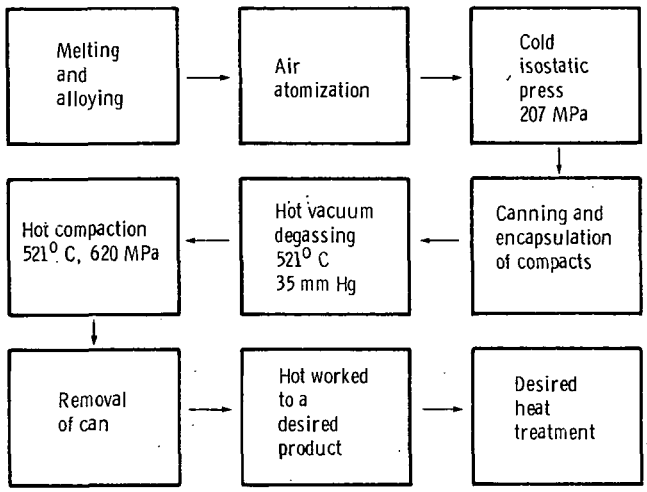

Figure 1. - Schematic of the powder metallurgy process.

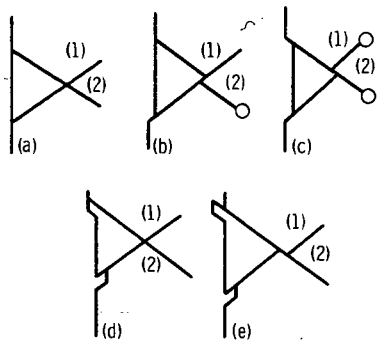

Figure 2. - Cottrell-Hull model for formation of intrusions and extrusions. Operation of two slip bands. (b) and (c) represent forward cycle, (d) and (e) reverse cycle (36).

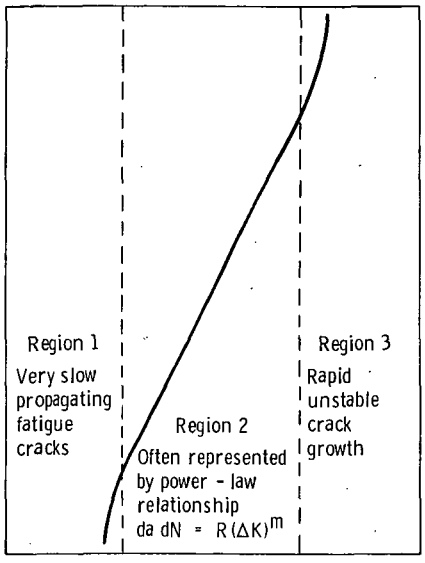

Figure 3. - Schematic of crack growth regions.

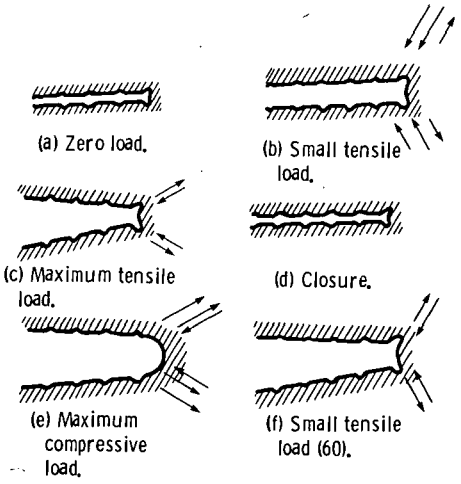

Figure 4. - Plastic-blunting model of FCP.

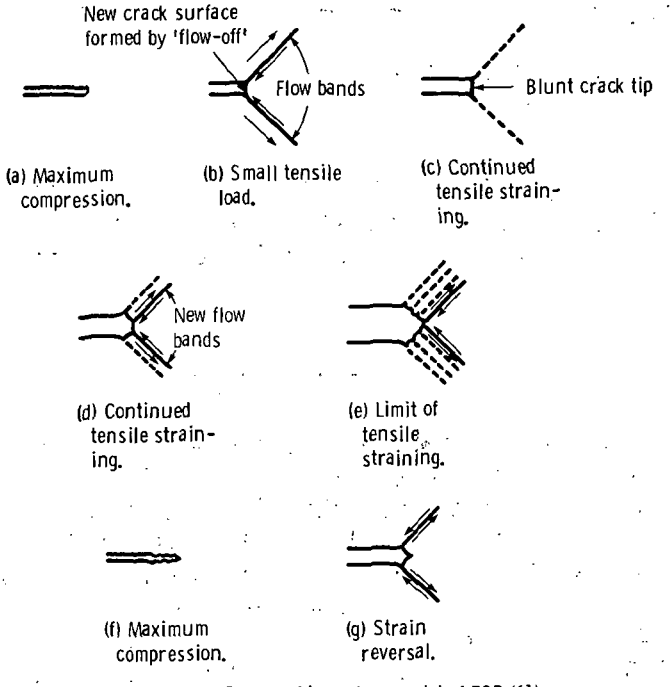

Figure 5. - Tomkins-Biggs model of FCP (61).

1. Report No.	2. Government Accession No.	3. Recipient's Catalog No.
NASA TM-83626		

4. Title and Subtitle	5. Report Date
Review of the Effects of Microstructure on Fatigue in Aluminum Alloys	April 1984
	6. Performing Organization Code: 505-33-22
7. Author(s): Jack Telesman	8. Performing Organization Report No.: E-2061
	10. Work Unit No.
9. Performing Organization Name and Address: National Aeronautics and Space Administration, Lewis Research Center, Cleveland, Ohio 44135	11. Contract or Grant No.
	13. Type of Report and Period Covered: Technical Memorandum
12. Sponsoring Agency Name and Address: National Aeronautics and Space Administration, Washington, D.C. 20546	14. Sponsoring Agency Code

15. Supplementary Notes

This report is part of a thesis submitted in partial fulfillment of the requirements for a Master's degree from the University of Cincinnati, Cincinnati, Ohio.

16. Abstract

Literature survey was conducted to determine the effects of different microstructural features and different load histories on fatigue crack initiation and propagation of aluminum alloys. Comparison of microstructure and monotonic and cyclic properties between powder metallurgy (P/M) and ingot metallurgy (I/M) alloys is presented. The two alloys that are representative of each process on which the comparison is focused are X7091 and 7050. Included in the report is a detailed description of the microstructure produced through the P/M and I/M processes. The effect of each pertinent microstructural feature on monotonic and cyclic properties, such as yield strength, toughness, crack initiation and propagation is discussed. Also discussed are the proposed mechanisms for crack initiation and propagation, as well as the effects of aggressive environments on these cyclic properties. Included is a discussion of the effects of variable amplitude loading on fatigue crack propagation and the various models proposed to predict load interaction effects.

17. Key Words (Suggested by Author(s))	18. Distribution Statement
Fatigue; Aluminum; Microstructure; Crack propagation; Spectrum loading; Crack initiation; Powder metallurgy; Ingot metallurgy	Unclassified - unlimited STAR Category 26

19. Security Classif. (of this report)	20. Security Classif. (of this page)	21. No. of pages	22. Price*
Unclassified	Unclassified		

*For sale by the National Technical Information Service, Springfield, Virginia 22161

National Aeronautics and
Space Administration

Washington, D.C.
20546

Official Business
Penalty for Private Use, $300

SPECIAL FOURTH CLASS MAIL
BOOK

Postage and Fees Paid
National Aeronautics and
Space Administration
NASA-451

NASA

POSTMASTER: If Undeliverable (Section 158
Postal Manual) Do Not Return